# Characterization of MJO-related upper tropospheric hydrological processes using MLS

Michael J. Schwartz,[1] Duane E. Waliser,[1] Baijun Tian,[2] Dong L. Wu,[1] Jonathan H. Jiang,[1] and William G. Read[1]

Received 15 February 2008; revised 12 March 2008; accepted 24 March 2008; published 26 April 2008.

[1] This study quantifies Madden-Julian Oscillation (MJO)-related hydrological variability in the upper troposphere/lower stratosphere (UT/LS) using Aura Microwave Limb Sounder (MLS) cloud ice water content (IWC) and water vapor ($H_2O$). In a composite of six boreal-winter MJO events, the UT/LS IWC anomaly is strongly positively correlated with the convection (TRMM rainfall) anomaly. IWC anomalies range from ±2 mg/m$^3$ at 215 hPa to ±0.08 mg/m$^3$ at 100 hPa. The UT/LS $H_2O$ anomaly has an eastward-tilting structure similar to the previous-documented temperature structure, but the $H_2O$ maximum lags the temperature maximum by about a week. The $H_2O$ anomaly is positively correlated with the convection anomaly in the UT (261 hPa) and LS (68 hPa) but negatively correlated with the convection anomaly near the tropopause (100 hPa). This analysis provides a multi-parameter construct useful in validating and improving the parameterization of convection, clouds and cloud microphysics in MJO modeling. **Citation:** Schwartz, M. J., D. E. Waliser, B. Tian, D. L. Wu, J. H. Jiang, and W. G. Read (2008), Characterization of MJO-related upper tropospheric hydrological processes using MLS, *Geophys. Res. Lett.*, *35*, L08812, doi:10.1029/2008GL033675.

## 1. Introduction

[2] The Madden-Julian Oscillation (MJO) is the dominant form of intraseasonal variability in the Tropics [*Madden and Julian*, 1994] and it impacts a wide range of phenomena, such as El Niño/La Niña, Asian-Australian monsoons, mid-latitude weather, tropical cyclones, and atmospheric composition [*Tian et al.*, 2008, 2007; *Waliser and Lau*, 2005]. To date, the large-scale MJO convection and circulation characteristics have been relatively well documented and in some cases understood [e.g., *Hendon and Salby*, 1994]. For the most part, these studies have focused on quantities such as upper and lower level winds, outgoing longwave radiation and precipitation, and surface heat budget processes. In recent years, a number of studies have also documented aspects of the MJO's vertical structure [e.g., *Myers and Waliser*, 2003; *Sperber*, 2003; *Kiladis et al.*, 2005; *Lin et al.*, 2005; *Tian et al.*, 2006; *Wong and Dessler*, 2007]. For example, in the work by *Tian et al.* [2006], Atmospheric Infrared Sounder (AIRS) [*Susskind et al.*, 2006] temperature and water vapor profiles were used to document the evolution of the moist thermodynamic vertical structure of the MJO. A notable limitation of this study as well as the other studies cited, with the exception of *Wong and Dessler* [2007], is that the data sources of water vapor information above ~300 hPa exhibit considerable uncertainty, lack sensitivity and/or are based on model-derived information. In addition, still missing in the characterization of the upper-tropospheric (UT) hydrological cycle of the MJO is a quantification of other hydrological properties (e.g., hydrometeor budgets, cloud ice/water, transports, etc).

[3] In this study, we use the water vapor ($H_2O$) and cloud ice water content (IWC) products from the Microwave Limb Sounder (MLS) [*Waters et al.*, 2006] on the Aura satellite to quantify the variation of upper-tropospheric/lower-stratospheric (UT/LS) humidity and cloud ice associated with the MJO. These products are now available for a more than three year period, filling significant gaps in our measurement capability and allowing a more complete characterization of the atmospheric hydrological cycle associated with the MJO. Quantitative profiling of these hydrological parameters is particularly important, as global climate and weather forecast models exhibit considerable shortcomings in the representation of the MJO [*Slingo et al.*, 1996; *Sperber et al.*, 2000; *Waliser et al.*, 2003b; *Lin et al.*, 2006; *Zhang et al.*, 2006]. Model deficiencies in regards to the MJO are thought to arise from gaps in our understanding of, and coupling between, cumulus convection, the planetary boundary layer, cloud-radiation processes, and possibly even microphysical processes and ocean surface temperature feedbacks [*Slingo et al.*, 2005]. Having a better characterization of the hydrological cycle in the UT will provide valuable model constraints on parametrized processes such as the degree of $H_2O$ supersaturation, auto-conversion rates of cloud to rainfall, as well as the contributions to "cloudiness" from cloud fraction, mass and particle size. In combination, these factors can help determine and quantify potentially important feedbacks to the MJO, including the cloud-longwave feedback [e.g., *Lin and Mapes*, 2004] and the surface shortwave-SST feedback [e.g., *Wang and Xie*, 1998; *Waliser et al.*, 1999]. Apart from the specific intention to examine the MJO, this study may also contribute to the stratospheric hydration problem, as the MJO modulates both convective injection of moisture into the tropical tropopause layer (TTL) and circulation between low and mid-latitudes [*Eguchi and Shiotani*, 2004; *Wong and Dessler*, 2007].

## 2. Data and Methodology

[4] This study uses MLS v1.5 $H_2O$ and IWC [*Livesey*, 2005]. $H_2O$ [*Read et al.*, 2007] is retrieved on 6-surfaces-per-decade of pressure from 316−0.1 hPa, and its overall

[1]Jet Propulsion Laboratory, California Institute of Technology, Pasadena, California, USA.
[2]Joint Institute for Regional Earth System Science and Engineering, University of California, Los Angeles, California, USA.


0094-8276/08/2008GL033675$05.00

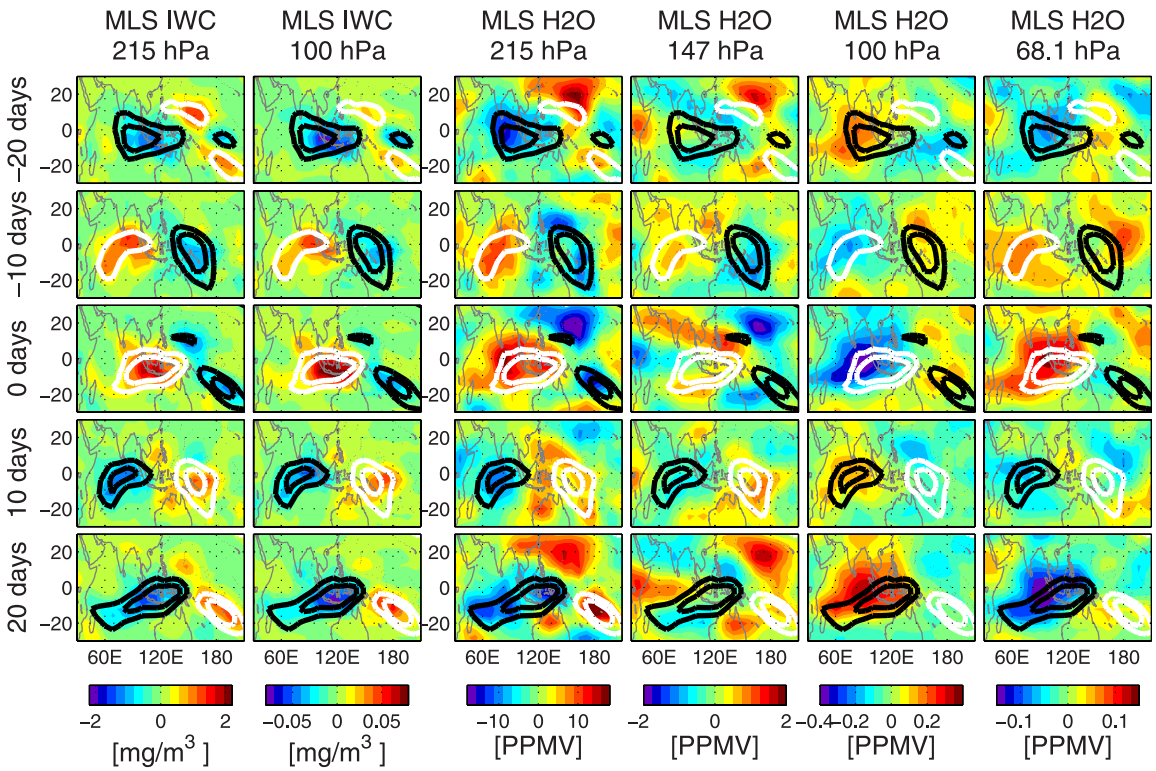


**Figure 1.** Composite MLS IWC and $H_2O$ 30–90 day variability. Similarly-averaged TRMM rainfall is shown by contours: +1 and +2 mm/day in white and −1 and −2 mm/day in black. 5 of 11 pentads are shown, and maps are limited to 30°S–30°N, 32°E–152°W.

accuracy is estimated to be about a factor of two. In the tropics, it has vertical resolution of ∼2 km at 316 hPa, degrading to ∼3 km at 100 hPa and ∼5 km at 46 hPa, and horizontal resolution of 7 km and ∼200 km across and along-track, respectively. IWC, screened as recommended by *Wu et al.* [2008], is retrieved on 12 surfaces per decade of pressure (∼1.3-km spacing) from 261–68 hPa, and should be interpreted as an average over a volume centered at the measurement point, with extent ∼3 km in vertical, ∼3 km across-track and ∼300 km along-track. V1.5 underestimates high IWC values (≳50 mg/m$^3$) at pressures greater than 147 hPa by up to 50% compared to the improved, v2.2 product, but the spatial and temporal morphology of the two products is generally similar, and consistent, in preliminary comparisons, with CloudSat [*Wu et al.*, 2008] (see also D. Waliser et al., Cloud ice: A climate model challenge with signs and expectations of progress, submitted to *Journal of Geophysical Research*, 2008). The v1.5 IWC noise floor is at ∼5 mg/m$^2$ at 261 hPa and ∼0.5 mg/m$^2$ at 100 hPa. Temperatures used are from the Goddard Earth Observing System Data Assimilation System (GEOS-4) [*Bloom et al.*, 2005]. The Tropical Rainfall Measuring Mission (TRMM) merged-infrared 3B42 precipitation product [*Huffman et al.*, 2007] is used to identify the magnitude and phase of MJO events.

[5] For the MJO analysis and composite procedure, we use the approach described in our previous papers [e.g., *Tian et al.*, 2006, 2007, 2008; *Waliser et al.*, 2003a]. Briefly, all the data are first binned into pentad values at a 8° long and 4° lat grid and then intraseasonal anomalies of the data are obtained by removing the annual and quasi-biennial (26-month) cycle and filtering through a 30–90-day band pass filter. To isolate the dominant structure of the MJO, an extended empirical orthogonal function (EEOF) [*Weare and Nasstrom*, 1982] is applied using time lags of ±5-pentads (i.e. 11 pentads total) on boreal winter rainfall for the region 30°S–30°N and 32°E–152°W [see Figure 1 of *Tian et al.* 2006]. While temporal filtering is done over the entire MLS data set, EEOF analysis and MJO events thereby identified are restricted to boreal-winter (Nov–Apr), when the eastward propagating form of the MJO is typically most active [e.g., *Waliser*, 2006]. MJO events are chosen based on the amplitude time series of the first EEOF mode of the rainfall anomaly. Supplementary material[1] shows the 11 time-lagged maps of this EEOF mode as well as the time-series of its projection, with the six selected MJO events indicated. A composite MJO cycle is obtained by averaging the 11-pentad blocks of IWC and $H_2O$ anomalies that are centered on the six selected events.

## 3. Results

[6] Figure 1 shows IWC and $H_2O$ MJO anomalies for a limited set of MLS retrieval levels, for latitudes 30°S–30°N, and longitudes 32°E–162°W. TRMM-rainfall anomaly contours (+1, +2 mm/day in white, −1, −2 mm/day in black) are also shown. Maps have been horizontally smoothed with nearest neighbors ([$\frac{1}{4}$, $\frac{1}{2}$, $\frac{1}{4}$] weighting) to suppress fine-structure variability arising from the limited

[1] Auxiliary materials are available in the HTML. doi:10.1029/2008GL033675.

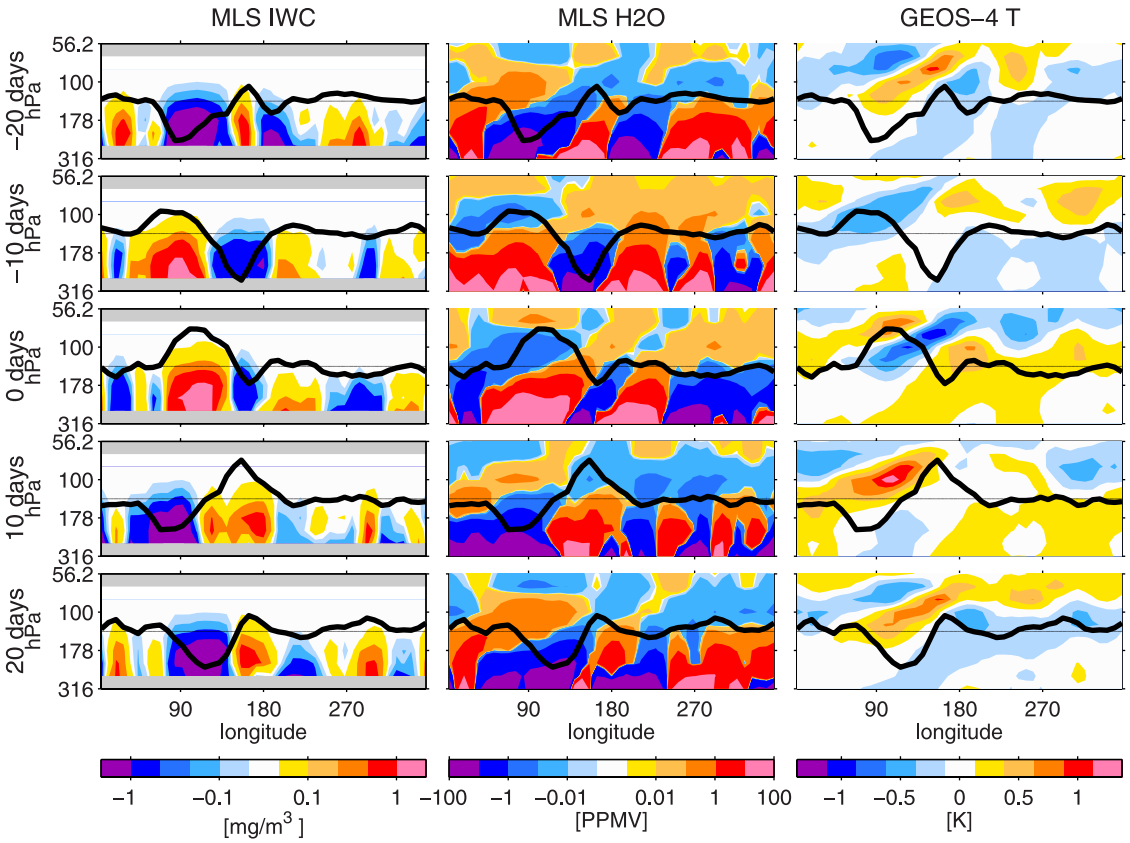


**Figure 2.** Composite MLS IWC (left panel), $H_2O$ (middle panel) and GEOS-4 temperature (right panel) 30–90 day anomalies averaged from 10°N to 10°S. Solid black lines are TRMM rainfall anomalies, with axes limits at ±3 mm/day. The color levels for both $H_2O$ and IWC are on logarithmic scales in magnitude. $H_2O$ has one color per decade of volume mixing ratio, with magnitudes less than 0.001 ppm in white. IWC has 3 colors per decade of density, with magnitudes less than 0.046 in white. The horizontal axis of each strip is longitude, covering the entire equator.

statistics of six events. No smoothing is done in the vertical direction. Anomalies propagate eastward from the Indian Ocean into the western Pacific at a rate of ~40° of equatorial longitude in 10 days, corresponding to the typical MJO propagation speed (~5 m/s).

[7] IWC anomalies at retrieval levels up to 100 hPa are highly positively correlated with convection anomalies and, therefore, with one another. 147 hPa IWC anomalies have correlation coefficients greater than 0.8 with anomalies at all other retrieval levels from 215 hPa to 100 hPa. The correlation of IWC with TRMM rainfall is 0.5 at 261 hPa, 0.7 at 147 hPa and 0.6 at 100 hPa. The magnitudes of these IWC anomalies drops by a factor of 50 from 261 hPa to 100 hPa, with peak anomalous values (given the applied smoothing) of ~±2 mg/m$^3$ at 215 hPa, ~±0.8 mg/m$^3$ at 147 hPa and ~±0.08 mg/m$^3$ at 100 hPa.

[8] No phase lag between IWC and TRMM convection is evident in Figure 1. Ice densities of cirrus outflow which remains aloft after convective events are small compared to those of convective cores and are generally below the MLS sensitivity thresholds (1.2–1.8 mg/m$^3$ at 215 hPa, 0.1–0.15 mg/m$^3$ at 100 hPa). Also, MLS 240-GHz radiances, on which v1.5 IWC is based, are relatively insensitive to small cirrus ice particles [*Wu and Jiang*, 2004]. Furthermore, the 5-day resolution of pentad-averaging may obscure small time lags. The study of low-density and small-particle-size ice distributions associated with MJO will benefit as multi-year datasets from new instruments such as CALIPSO [*Winker et al.*, 2004] and CloudSat [*Stephens et al.*, 2002] become available.

[9] The right four columns of Figure 1 show MJO anomalies of MLS $H_2O$. $H_2O$ is positively correlated with TRMM rainfall at 316 hPa and 215 hPa and is negatively correlated with TRMM rainfall at 100 hPa [*Mote et al.*, 2000; *Tian et al.*, 2006; *Wong and Dessler*, 2007]. $H_2O$ at 68 hPa is again positively correlated with TRMM rainfall, and this correlation persists when $H_2O$ is interpolated to isentropic surfaces (not shown), an indication that this $H_2O$ anomaly in the LS is not simply due isentropic movement of water vapor relative to pressure surfaces.

[10] Off-equatorial $H_2O$ anomalies associated with the MJO's equatorial Rossby wave gyres [e.g., *Hendon and Salby*, 1994; *Tian et al.*, 2007] are evident, particularly at 215 hPa and 147 hPa. Low-pressure subtropical gyres east of the enhanced equatorial convection are associated with negative $H_2O$ anomalies while high-pressure subtropical gyres west of the enhanced equatorial convection tend to have positive $H_2O$ anomalies.

[11] Figure 2 shows equatorial (10°N–10°S average) pressure-longitude plots of MJO anomalies in MLS IWC and $H_2O$ and in GEOS-4 temperature, for all longitudes. IWC anomalies propagate eastward from Africa into the

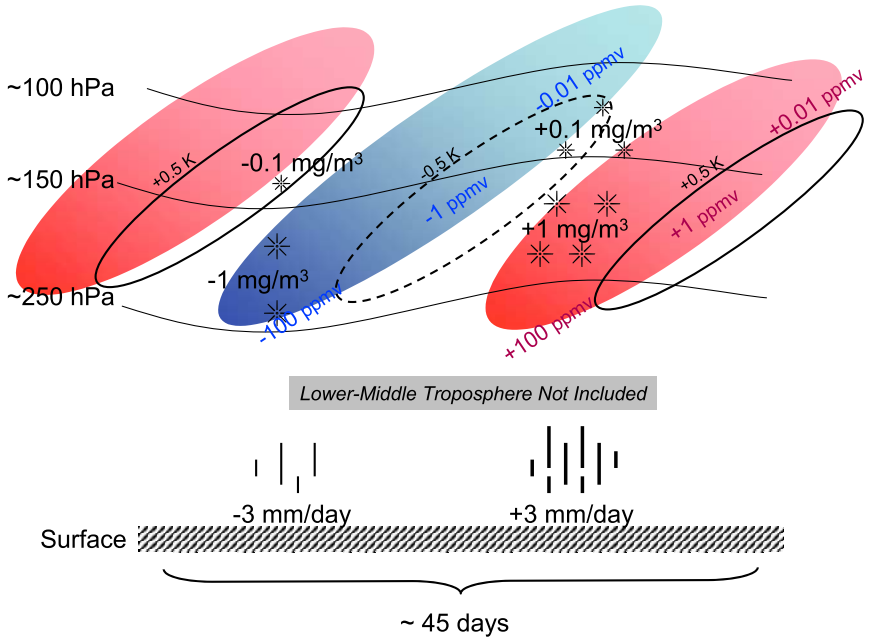


**Figure 3.** MJO equatorial (10°N–10°S) hydrological structure schematic. $H_2O$ anomalies are shaded pink/blue and temperature anomalies are solid/dashed lines, positive/negative respectively. The magnitudes of IWC anomalies are indicated by the density of snowflake symbols.

Western Pacific, in phase with TRMM rainfall anomalies (contour lines), with anomalies reaching ±1 mg/m$^3$ up to 178 hPa in the Indian Ocean and western Pacific. At 316 hPa, GEOS-4 temperature and MLS $H_2O$ are both positively correlated with the convection anomaly in the eastern hemisphere. The temperature anomaly between 178 hPa and 68 hPa has structure tilting eastward with increasing height, a well-documented feature of the MJO [e.g., *Kiladis et al.*, 2005; *Tian et al.*, 2006]. GEOS-4 temperature shows a sharpening of the tropopause above the positive convection anomaly, cooling at 100 hPa and warming at 68 hPa and in the lower troposphere. At 178–68 hPa, $H_2O$ also has an eastward tilting vertical structure similar to that seen in temperature, but the $H_2O$ anomaly lags the temperature anomaly by 8–10 days from 215–147 hPa and by 5–6 days at 121 hPa and 100 hPa. MJO modulation of $H_2O$ at 215 hPa and deeper in the troposphere is controlled by direct convective injection of moist air, while at 100 hPa dry and cold anomalies above enhanced convection are positively correlated, but causal relationships are uncertain [e.g., *Mote et al.*, 2000; *Wong and Dessler*, 2007].

## 4. Conclusions

[12] The combination of the MLS IWC and $H_2O$ products provide a previously-unavailable picture of UT/LS hydrological processes associated with the MJO. Intraseasonal (30–90 day) variability in MLS IWC and $H_2O$ and GEOS-4 temperature was composited over six boreal-winter MJO events identified with a TRMM-rainfall-based index. A schematic of the equatorial composite anomalous structure of IWC, $H_2O$, temperature and rainfall associated with the MJO is summarized in Figure 3. IWC anomalies between 261 hPa and 100 hPa are spatially and temporally highly positively correlated with convective anomalies, with magnitudes ranging from ±2 mg/m$^3$ at 215 hPa to ±0.08 mg/m$^3$ at 100 hPa. The UT/LS $H_2O$ anomaly has an eastward-tilting structure similar to the previous-documented temperature structure but $H_2O$ lags temperature by 8–10 days from 215–147 hPa and by 5–6 days at 121–100 hPa. The $H_2O$ anomaly is positively correlated with the convection anomaly in the UT (261hPa) and LS (68 hPa) but negatively correlated with the convection anomaly near the tropopause (100 hPa).

[13] Given the great difficulties that GCMs still have at reproducing the MJO, both in weather forecast and climate simulation contexts, it is imperative that additional observational constraints be developed and applied. Since it is thought that correct parameterization of convection, and possibly clouds and cloud microphysics, lie at the heart of the MJO simulation problem, the multi-parameter view of the hydrological cycle of the MJO that is coalesced into Figure 3 can provide such a constraint. It includes key features of the cloud-radiation-dynamical interactions that are thought to be important to a realistic representation of the MJO. Moreover, due to the widespread vertical mixing associated with the disturbed phase of the MJO and the associated influence on atmospheric composition [e.g., *Wong and Dessler*, 2007; *Tian et al.*, 2007, 2008], it will be important to continue to develop multi-parameter validation constructs. The A-train sensors [*Stephens et al.*, 2002] including MLS, CloudSat and CALIPSO provide a suite of relevant, nearly-collocated measurements that will be particularly valuable to this end.

[14] **Acknowledgments.** Work at the Jet Propulsion Laboratory, California Institute of Technology, was done under contract with the

National Aeronautics and Space Administration. Copyright 2008 California Institute of Technology, Government sponsorship acknowledged.

## References


Bloom, S., et al. (2005), Documentation and validation of the Goddard Earth Observing System (GEOS) Data Assimilation System–Version 4, *NASA TM-104606*, vol. 26, 2005, 1–157.

Eguchi, N., and M. Shiotani (2004), Intraseasonal variations of water vapor and cirrus clouds in the tropical upper troposphere, *J. Geophys. Res.*, *109*, D12106, doi:10.1029/2003JD004314.

Hendon, H., and M. Salby (1994), The life cycle of the Madden–Julian oscillation, *J. Atmos. Sci.*, *51*, 2225–2237.

Huffman, G., R. Adler, D. Bolvin, G. Gu, E. Nelkin, K. Bowman, Y. Hong, E. Stocker, and D. Wolff (2007), The TRMM multisatellite precipitation analysis (TMPA): Quasi-global, multiyear, combined-sensor precipitation estimates at fine scales, *J. Hydrometeorol.*, *8*, 38–55, doi:10.1175/JHM560.1.

Kiladis, G., K. Straub, and P. Haertel (2005), Zonal and vertical structure of the Madden–Julian oscillation, *J. Atmos. Sci.*, *62*, 2790–2809.

Lin, J., and B. Mapes (2004), Radiation budget of the tropical intraseasonal oscillation, *J. Atmos. Sci.*, *61*, 2050–2062.

Lin, J., M. Zhang, and B. Mapes (2005), Zonal momentum budget of the Madden–Julian Oscillation: The source and strength of equivalent linear damping, *J. Atmos. Sci.*, *62*, 2172–2188.

Lin, J., et al. (2006), Tropical intraseasonal variability in 14 IPCC AR4 climate models. Part I: Convective signals, *J. Clim.*, *19*, 2665–2690.

Livesey, N. J. (2005), Data quality document for the EOS MLS version 1.5 level 2 dataset, technical report, Jet Propul. Lab., Pasadena, Calif.

Madden, R., and P. Julian (1994), Observations of the 40–50–day tropical oscillation – a review, *Mon. Weather Rev.*, *122*, 814–837.

Mote, P. W., H. L. Clark, T. J. Dunkerton, R. S. Harwood, and H. C. Pumphrey (2000), Intraseasonal variations of water vapor in the tropical upper troposphere and tropopause region, *J. Geophys. Res.*, *105*, 17,457–17,470.

Myers, D., and D. Waliser (2003), Three-dimensional water vapor and cloud variations associated with the Madden–Julian oscillation during northern hemisphere winter, *J. Clim.*, *16*, 929–950.

Read, W. G., et al. (2007), Aura Microwave Limb Sounder upper tropospheric and lower stratospheric $H_2O$ and relative humidity with respect to validation, *J. Geophys. Res.*, *112*, D24S35, doi:10.1029/2007JD008752.

Slingo, J., et al. (1996), Intraseasonal oscillations in 15 atmospheric general circulation models: Results from an AMIP diagnostic subproject, *Clim. Dyn.*, *12*, 325–357.

Slingo, J., P. Inness, and K. Sperber (2005), Modeling, in *Intraseasonal Variability in the Atmosphere-Ocean Climate System*, edited by D. Waliser and W. Lau, pp. 361–388, Springer, New York.

Sperber, K. (2003), Propagation and the vertical structure of the Madden–Julian oscillation, *Mon. Weather Rev.*, *131*, 3018–3037.

Sperber, K., J. Slingo, and H. Annamalai (2000), Predictability and the relationship between subseasonal and interannual variability during the Asian summer monsoon, *Q. J. R. Meteorol. Soc.*, *126*, 2545–2574.

Stephens, G., et al. (2002), The CloudSat mission and the A-train, *Bull. Am. Meteorol. Soc.*, *83*, 1771–1790.

Susskind, J., C. Barnet, J. Blaisdell, L. Iredell, F. Keita, L. Kouvaris, G. Molnar, and M. Chahine (2006), Accuracy of geophysical parameters derived from Atmospheric Infrared Sounder/Advanced Microwave Sounding Unit as a function of fractional cloud cover, *J. Geophys. Res.*, *111*, D09S17, doi:10.1029/2005JD006272.

Tian, B., D. Waliser, E. Fetzer, B. Lambrigtsen, Y. Yung, and B. Wang (2006), Vertical moist thermodynamic structure and spatial–temporal evolution of the MJO in AIRS observations, *J. Atmos. Sci.*, *63*, 2462–2485.

Tian, B., Y. Yung, D. Waliser, T. Tyranowski, L. Kuai, E. Fetzer, and F. Irion (2007), Intraseasonal variations of the tropical total ozone and their connection to the Madden-Julian oscillation, *Geophys. Res. Lett.*, *34*, L08704, doi:10.1029/2007GL029471.

Tian, B., et al. (2008), Does the Madden-Julian oscillation influence aerosol variability?, *J. Geophys. Res.*, doi:10.1029/2007JD009372, in press.

Waliser, D., and W. Lau (2005), *Intraseasonal Variability in the Atmosphere-Ocean Climate System*, Springer, New York.

Waliser, D., K. Lau, and J. Kim (1999), The influence of coupled sea surface temperatures on the Madden–Julian oscillation: A model perturbation experiment, *J. Atmos. Sci.*, *56*, 333–358.

Waliser, D., R. Murtugudde, and L. Lucas (2003a), Indo-Pacific Ocean response to atmospheric intraseasonal variability: 1. Austral summer and the Madden-Julian oscillation, *J. Geophys. Res.*, *108*(C5), 3160, doi:10.1029/2002JC001620.

Waliser, D., et al. (2003b), AGCM simulations of intraseasonal variability associated with the Asian summer monsoon, *Clim. Dyn.*, *21*, 423–446.

Waliser, D. E. (2006), Intraseasonal variability, in *The Asian Monsoon*, edited by B. Wang, chapter 5, pp. 203–257, Springer, New York.

Wang, B., and X. Xie (1998), Coupled modes of the warm pool climate system. Part 1: The role of air–sea interaction in maintaining Madden–Julian oscillation, *J. Clim.*, *11*, 2116–2135.

Waters, J., et al. (2006), The Earth Observing System Microwave Limb Sounder (EOS MLS) on the Aura Satellite, *IEEE Trans. Geosci. Remote Sens.*, *44*, 1075–1092.

Weare, B., and J. Nasstrom (1982), Examples of extended empirical orthogonal function analyses, *Mon. Weather Rev.*, *110*, 481–485.

Winker, D., W. Hunt, and C. Hostetler (2004), Status and performance of the CALIOP lidar, *Proc. SPIE Int. Soc. Opt. Eng.*, *5575*, 8–15.

Wong, S., and A. E. Dessler (2007), Regulation of $H_2O$ and CO in tropical tropopause layer by the Madden-Julian oscillation, *J. Geophys. Res.*, *112*, D14305, doi:10.1029/2006JD007940.

Wu, D. L., and J. H. Jiang (2004), EOS MLS algorithm theoretical basis for cloud measurements, *Tech. rep. D-19299*, Jet Propul. Lab., Pasadena, Calif.

Wu, D. L., et al. (2008), Validation of the Aura MLS cloud ice water content (IWC) measurements, *J. Geophys. Res.*, doi:10.1029/2007JD008931, in press.

Zhang, C., M. Dong, S. Gualdi, H. Hendon, E. Maloney, A. Marshall, K. Sperber, and W. Wang (2006), Simulations of the Madden–Julian oscillation in four pairs of coupled and uncoupled global models, *Clim. Dyn.*, *27*, 573–592.


J. H. Jiang, W. G. Read, M. J. Schwartz, D. E. Waliser, and D. L. Wu, Jet Propulsion Laboratory, California Institute of Technology, 4800 Oak Grove Drive, Pasadena, CA 91109, USA. (michael.j.schwartz@jpl.nasa.gov)

B. Tian, Joint Institute for Regional Earth System Science and Engineering, University of California, Los Angeles, CA 90024, USA.